How to cite: *Angew. Chem. Int. Ed.* **2022,** *61,* e202205453
International Edition: doi.org/10.1002/anie.202205453
German Edition: doi.org/10.1002/ange.202205453

Metal-Organic Frameworks

2D MOF with Compact Catalytic Sites for the One-pot Synthesis of 2,5-Dimethylfuran from Saccharides via Tandem Catalysis

Qiang Deng, Xuemeng Hou, Yao Zhong, Jiawei Zhu, Jun Wang, Jianxin Cai, Zheling Zeng, Ji-Jun Zou, Shuguang Deng,* Tatchamapan Yoskamtorn, and Shik Chi Edman Tsang**

Abstract: One pot synthesis of 2,5-dimethylfuran (2,5-DMF) from saccharides under mild conditions is of importance for the production of biofuel and fine chemicals. However, the synthesis requires a multitude of active sites and suffers from slow kinetics due to poor diffusion in most composite catalysts. Herein, a metal-acid functionalized 2D metal-organic framework (MOF; Pd/NUS-SO_3H), as an ultrathin nanosheet of 3–4 nm with Lewis acid, Brønsted acid, and metal active sites, was prepared based on the diazo method for acid modification and subsequent metal loading. This new composite catalyst gives substantially higher yields of DMF than all reported catalysts for different saccharides (fructose, glucose, cellobiose, sucrose, and inulins). Characterization suggests that a cascade of reactions including polysaccharide hydrolysis, isomerization, dehydration, and hydrodeoxygenation takes place with rapid molecular interactions.

[*] Dr. Q. Deng, Dr. X. Hou, Dr. Y. Zhong, J. Zhu, Prof. J. Wang, Prof. J. Cai, Prof. Z. Zeng
School of Chemistry and Chemical Engineering,
Nanchang University
No. 999 Xuefu Avenue, Nanchang 330031 (P. R. China)
E-mail: dengqiang@ncu.edu.cn
Prof. J.-J. Zou
School of Chemical Engineering and Technology,
Tianjin University
No.92 Weijin Road, Tianjin 300072 (P. R. China)
Prof. S. Deng
School for Engineering of Matter, Transport and Energy,
Arizona State University
551 E. Tyler Mall, Tempe, AZ 85287 (USA)
E-mail: Shuguang.Deng@asu.edu
Dr. T. Yoskamtorn, Prof. S. C. E. Tsang
Wolfson Catalysis Centre, Department of Chemistry,
University of Oxford
Oxford OX1 3QR (UK)
E-mail: edman.tsang@chem.ox.ac.uk

Introduction

Upgrading lignocellulose into biofuel and fine chemicals is a promising route to a sustainable future economy. 2,5-Dimethylfuran (2,5-DMF) is regarded as an important biomass-based compound that can be used not only as a biofuel but also as a building block for various high value-added fine chemicals, such as p-xylene, linear ketone/alcohol, and pyrrole.[1–3] Although the synthesis of 2,5-DMF from saccharides (such as fructose, glucose, cellobiose, sucrose, and inulin) via a two-step method, which consists of acid-catalyzed hydrolysis, isomerization, and dehydration of saccharides to intermediate 5-hydroxymethylfurfural (5-HMF) and subsequent metal-catalyzed hydrodeoxygenation of 5-HMF into 2,5-DMF,[4–10] can achieve theoretically high yield, the intermediate 5-HMF isolation before its hydrodeoxygenation increases the energy consumption and decreases the final 2,5-DMF yield.[11,12] In contrast, one-pot conversion of saccharides to 2,5-DMF without 5-HMF isolation is more desirable due to the greater energy integration and higher production efficiency.

Early experiments proposed a two-step method containing dehydration of fructose to 5-HMF with a yield of approximately 80 % at 130–150 °C and subsequent hydrodeoxygenation with a overall 2,5-DMF yield of 20–50 % at 150–220 °C over a mixture of acid and metal catalysts (e.g., $ZnCl_2$ + Pd/C and acidic ionic liquid + Ru/C).[8,13–15] Unfortunately, the two-step reaction systems suffered from long reaction time, low 2,5-DMF yield, and corrosivity of homogeneous acids. Subsequently, several solid acid-supported metal catalysts (e.g., Pd/UiO-66 + C-SO_3H, Pd/UiO-66@sulfonated graphene oxide, and Pd/Cr-MIL-101-SO_3H) were developed for the one-pot upgrading of fructose to 2,5-DMF at 150–220 °C.[16–20] However, their catalytic activities were limited by the slow diffusion rate of the organics within the 3D catalysts, especially for macromolecular compounds. More unfortunately, the focused feedstock was mainly simple fructose, but other low-activity monosaccharides (i.e. glucose), disaccharides (i.e. cellobiose and sucrose) and polysaccharides (such as inulin) were not attempted. Particularly, the direct saccharide conversion to 2,5-DMF remains more challenging because of the extra steps for saccharides hydrolysis and glucose isomerization. Therefore, developing a multifunctional tandem catalyst with a rapid molecular intereactions with compact active sites at high density is critical to promoting a desirable continuous reaction route.

As a new 2-dimensional (2D) material, 2D MOF with controlled thickness of a few nanometers and highly exposed

active sites has been investigated in the fields of gas separation, catalysis, energy storage, electronic sensors, and biomedicine.[21–28] In the field of thermocatalysis, using 2D MOF to host transition metal nanoparticles has been reported for the catalytic oxidation and catalytic hydrogenation reactions.[29–34] However, these reactions are simply metal-catalyzed reactions. The catalytic reactions such as hydrolysis, isomerization, and dehydration reactions that combine metal and acid-base catalytic functions of the host structure are rarely reported. It is hypothesized that 2D MOF-supported strong acid groups and metal sites with lower diffusion distances than 3D composite counterparts can strengthen the synergistic effect of acid catalysis and hydrogenation catalysis for 2,5-DMF reactions. The classical preparation of sulfonic acid-grafted MOF is direct synthesis from sulfonated ligands, but the sulfonic acid (SO_3H) groups often change the electron distribution of the ligand and cause a collapsed structure.[35,36] Because of the lack of a rational design methodology for locating SO_3H groups in the framework structure, strong acid-functionalized 2D MOFs have not been reported, not to mention the preparation of multi-functionalized metal-acid catalysts.

Herein, Pd-supported SO_3H-modified 2D MOF (Pd/NUS-SO_3H) with a 0.62 mmol g^{-1} Lewis acid density, 0.83 mmol g^{-1} Brønsted acid density, and 1.0 wt % Pd content is prepared for the first time by a diazo method using 4-aminobenzenesulfonic acid as a sulfonating agent and a subsequent incipient method using palladium chloride as the Pd precursor. Compared with 3DMOF-based catalyst (Pd/UiO-SO_3H), the prepared Pd/2D MOF-SO_3H exhibits much higher catalytic activity and 2,5-DMF selectivity by intensifying consecutive hydrolysis, isomerization, dehydration of saccharides, and hydrodeoxygenation of 5-HMF. Furthermore, the composite catalyst is stable after at least 4 recycles. To the best of our knowledge, this work represents the first effort to explore the synergistic catalysis of hydrogenation sites and acid sites for complex biomass conversion reactions based on the intrinsic characteristics of rapid diffusion of the 2D MOF structure.

Results and Discussion

Details of the catalyst synthesis and characterization are provided in the Supporting Information. As shown in Figure 1A, the 2D MOF NUS-8 (abbreviated as NUS) was prepared via a solvothermal method, and then used as the precursor for SO_3H-functionalized 2D MOF (NUS-SO_3H) by the diazo grafting of 4-aminobenzenesulfonic acid.[30,37,38] Subsequently, Pd- and SO_3H-modified 2D MOF (Pd/NUS-SO_3H) was synthesized through a simple impregnation method using palladium chloride as the Pd source, followed by reduction in H_2/Ar atmosphere. For comparison, Pd-supported NUS and active carbon (Pd/NUS, Pd/C) without

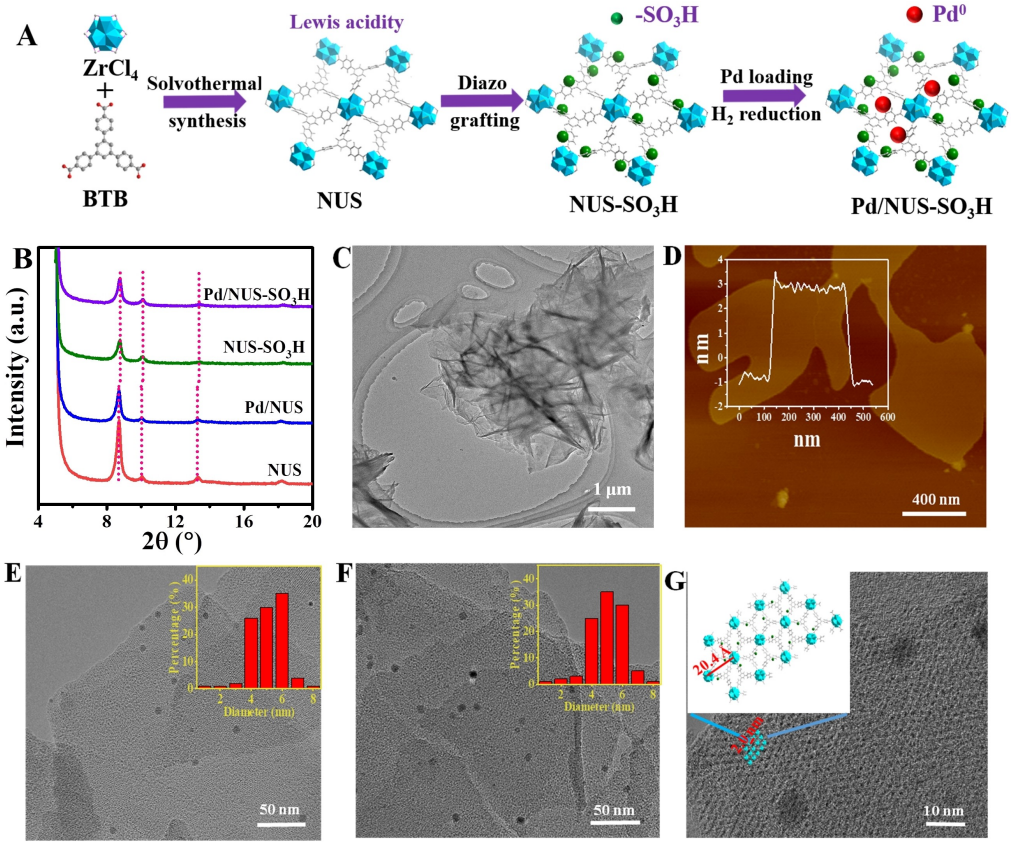

Figure 1. A) Synthesis of Pd/NUS-SO_3H; B) PXRD patterns of catalysts; C) TEM and D) AFM images of Pd/NUS-SO_3H; HRTEM images of E) Pd/NUS and (F, G) Pd/NUS-SO_3H.

acid functionalization were synthesized with the same method. Powder X-ray diffraction (PXRD) peaks for the NUS matched well with standard crystallographic data (No. 1567188) (Figure 1B), which implies that solid is highly crystalline. NUS is a stable 2D MOF nanosheets composed of hexanuclear Zr_6 clusters and 1,3,5-benzene-tribenzoate (BTB) ligand, and the 3D structure is inhibited via a formic acid-modulated effect during solvothermal synthesis.[30,34] ^{1}H-NMR spectrum of the digested NUS gives a formate: BTB molar ratio of 3 (Figure S1), which matches the formate-capped structure $Zr_6(\mu_3\text{-}O)_4(\mu_3\text{-}OH)_4(O_2CH)_6\text{-}(BTB)_2$.[34,38] However, the formate ions are unstable and can be removed by activation.[34,38] Elemental analysis results of activated NUS indicate that the C:Zr molar ratio of NUS (i.e., 9.05) is very close to the stoichiometrically expected value (i.e., 9) (Table S1). After functionalization, the composite catalyst possesses an approximately 1.0 wt % Pd content and 2.7 wt % S content (Table 1). Meanwhile, the C:Zr molar ratio increases to 10.19 due to the introduction of benzenesulfonic acid. Typical diffraction peaks of SO_3H-functionalized samples (including NUS-SO_3H and Pd/NUS-SO_3H) exhibited a slightly shift, which indicates the chemical grafting of SO_3H group causes a lattice shrink of 2D MOF and Pd species are simply supported on the host (Figure S2, Table S2). Transmission electron microscope (TEM) images confirmed that the catalyst was randomly stacked with 2D nanosheet structures (Figure 1C). Atomic force microscope (AFM) image indicated the unilaminar topological structure of the 2D MOF with a thickness of 3–4 nm (Figure 1D). The high-resolution TEM (HRTEM) images showed the size distribution of Pd nanoparticles for Pd/NUS and Pd/NUS-SO_3H of 4–6 nm (Figures 1D, E, F). The observed distance between adjacent Zr_6 clusters was about 2.0 nm, which is agreeable to the modeled structural (20.4 Å) of NUS (Figure 1G).[27,34] The high-angle annular dark-field scanning TEM (HAADF-STEM) micrograph and elemental mapping confirmed that the Pd nanoparticles and S element are evenly dispersed on the surface of the Pd/NUS-SO_3H (Figure S3).

The X-ray photoemission spectroscopy (XPS) Pd 3d spectra showed two peaks centered at 337.3 and 342.4 eV (the $3d_{5/2}$ and $3d_{3/2}$ signal of Pd^0) (Figure S4).[39] The Pd dispersity was also confirmed by temperature-programmed reduction (H_2-TPR) and H_2-D_2 exchange tests.[40,41] Pd/NUS and Pd/NUS-SO_3H possessed a similar Pd dispersity of approximately 20 % and generation capability of HD (Figures 2A, B, Table 1). It indicates they possess a similar H_2 activation ability, which is an important step in the reaction process. The S 2p XPS spectra can be deconvoluted into three peaks at 167.2, 167.7, and 168.5 eV (S–C, S–O, and S=O bonds)[37,42] (Figure S4). Meanwhile, Fourier Transform Infrared (FTIR) spectra indicated that, compared with the NUS, NUS-SO_3H and Pd/NUS-SO_3H show extra peaks at 635 cm^{-1} (S–O bond), 1032 and 1174 cm^{-1} (S=O bond) (Figure 2C).[37,42] During the diazo grafting process, 4-aminobenzenesulfonic acid was first formed benzenesulfonic acid-contained diazo salt by $NaNO_2$ oxidation and HCl mediation, and then it generates benzenesulfonic acid carbocation

Table 1: Physicochemical properties of catalysts.

Catalyst	Pd content [wt %]	S content [wt %]	S_{BET} [$m^2 g^{-1}$]	External surface area [$m^2 g^{-1}$]	Dispersion [%]	Lewis acid amount [mmol g^{-1}]	Brønsted acid amount[a] [mmol g^{-1}]
Pd/NUS	1.03	/	427.4	132.4	18.8	0.75	– (–)
Pd/NUS-SO_3H	0.96	2.75	229.6	206.3	19.8	0.62	0.83 (0.86)
Pd/UiO-SO_3H	1.02	2.62	531.2	20.5	18.7	0.65	0.78 (0.82)

[a] The data in parentheses are the theoretical value.

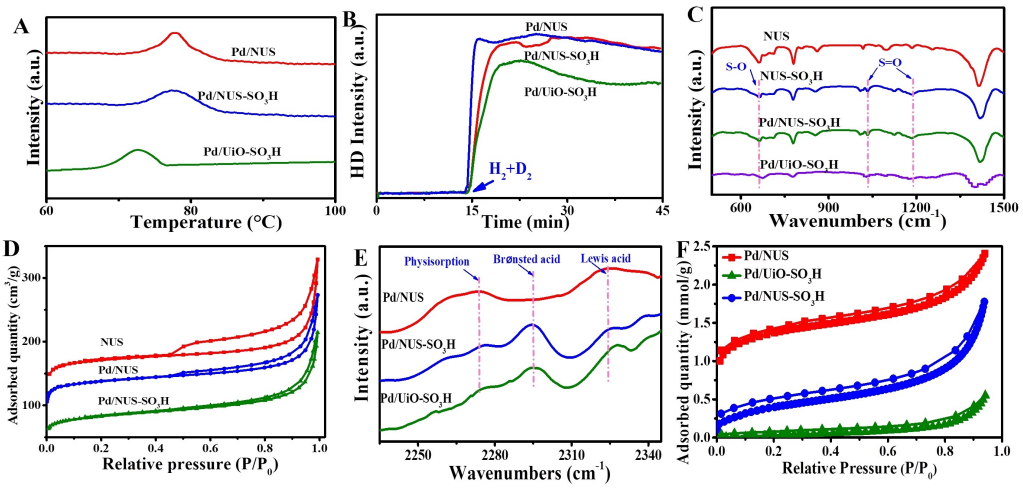

Figure 2. A) H_2-TPR; B) MS signals of HD generation during H_2-D_2 exchange test; C) FTIR spectra; D) N_2 adsorption-desorption isotherms; E) CD_3CN-adsorbed FTIR spectra; and F) cyclohexane adsorption/desorption isotherms of various catalysts.

after elimination of H_2O and N_2. Subsequently, the benzenesulfonic acid group was anchored on the carbon atom of the MOF host, accompanied by HCl elimination (Figure S5). The N_2 adsorption isotherms of NUS exhibit hybrid type I and IV curves with plateaus of 0.1–0.4 P/P_0 and hysteresis loops of 0.4–0.9 P/P_0, indicating the presence of micropores in the host and mesopores formed by nanosheet stacking (Figure 2D). NUS possess a large Brunauer–Emmett–Teller (BET) specific surface area of 556.2 $m^2 g^{-1}$, and external specific surface area of 102.8 $m^2 g^{-1}$ (Figure 2D, Table S1). The pore size distribution calculated using the nonlocal density functional theory (NLDFT) model reveals a pore size centered at 1.5 nm, which match well with the crystal structure (Figure S6).[30] Meanwhile, the Barrett–Joyner–Halenda (BJH) model suggests the existence of mesopores with pore size of 3.8 nm via the stacking of monolayers. The specific surface area and pore size are substantially reduced after the introduction of SO_3H groups and Pd nanoparticles (Table 1). Whereas, the external specific surface area is gradually increased. These results indicate the successful introduction of Pd nanoparticles and SO_3H groups on the external surface of 2D MOF.

As a reference, 3DMOF-based catalyst (Pd/UiO-SO_3H) with a 1.02 wt % Pd content, 18.7 % Pd dispersity, 2.62 wt % S content, and BET surface area of 531.2 $m^2 g^{-1}$ was synthesized via an identical procedure using 3DMOF (UiO-66) as the host (Figures 2, S6, S7, Table 1).[36,43] It possesses a compact structure with an external specific surface area of 20.5 $m^2 g^{-1}$.[36] Its PXRD pattern matches well with the reported data, confirming that the 3DMOF sample has the same crystal structure. IR spectra of the in situ chemisorbed CD_3CN were used to identify the acid properties (Figure 2E). The peaks at 2273 cm^{-1} can be attributed to physisorbed CD_3CN.[44,45] The IR spectrum of Pd/NUS showed pure Lewis acidity with a sole peak at 2325 cm^{-1}. Combined with the high crystallinity of Pd/NUS, the Lewis acid sites were ascribed to the coordination-unsaturated Zr^{4+} in the Zr_6 clusters after the removal of formate ion rather than the edge of the crystal.[30,38,43] The SO_3H-functionalized catalysts exhibited an additional peak at 2296 cm^{-1}, which is attributed to the Brønsted acidity. These catalysts possess Lewis and Brønsted acid densities of 0.62–0.75 mmol g^{-1} and 0.78–0.83 mmol g^{-1}, respectively.[44] The measured Brønsted acid density is consistent with the theoretical value calculated from the S content. The high density ensures abundant acidic sites for acid-catalyzed reactions. Meanwhile, the physical adsorption of cyclohexane was conducted in a gravimetric sorption analyzer (Figure 2F). Although Pd/NUS-SO_3H has a much lower specific area than that of Pd/UiO-SO_3H, it exhibits a faster adsorption rate and higher adsorption capacity due to the lamellar structure.[30,34]

5-HMF hydrodeoxygenation was initially conducted under isopropanol (IPA) solvent (Figure 3A). Control experiments show that only etherified 5-isopropoxymethyl furfural is obtained under an N_2 atmosphere, and only hydrogenated 2,5-bishydroxymethyl furan (2,5-BHMF) is observed under an H_2 atmosphere and water solvent (Figure S8). The etherification of the hydroxyl groups of 2,5-BHMF with IPA to 2,5-bis-isopropoxymethyl furan (2,5-BIMF) can weaken the C–O bond and accelerate the subsequent hydrogenolysis step. These intermediates were verified by gas chromatography-mass spectrometry (GC-MS) (Figure S9). Due to the mild reaction conditions, these catalysts have a high carbon balance above 98 %. In the temporal evolution curve of product distributions, the acid-functionalized Pd/NUS-SO_3H and Pd/UiO-SO_3H show an increase in 2,5-DMF concentration and an initial increase and then a decrease in 2,5-BHMF, 2,5-BIMF, and 2-isopropoxymethyl 5-methylfuran (2-IMMF) concentrations (Figures 3B, C). In comparison, Pd/NUS shows catalytic conversion with only hydrogenated 2,5-BHMF delivered, with no subsequent etherification and hydrogenolysis (Figure 3D). HMF is initially hydrogenated to 2,5-BHMF on Pd

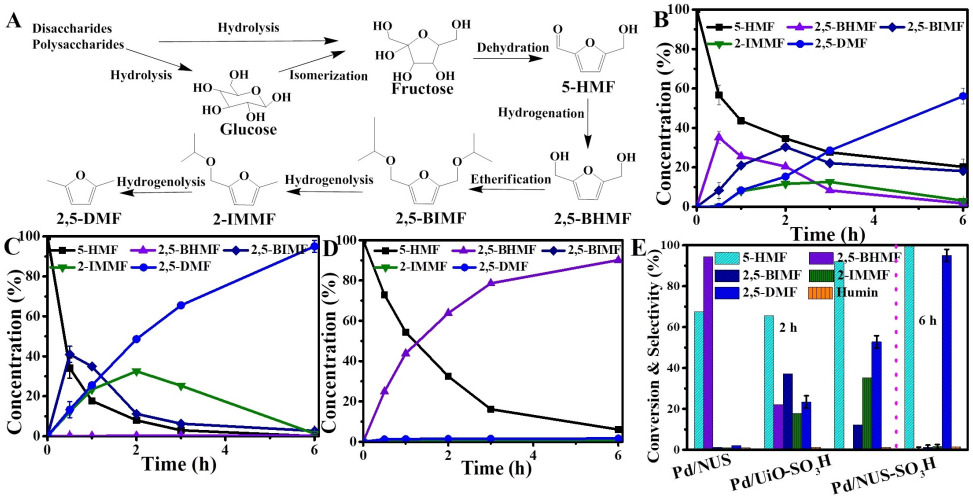

Figure 3. A) Reaction pathway of saccharides and 5-HMF to 2,5-DMF; Time-dependent product concentration of 5-HMF to 2,5-DMF over B) Pd/UiO-SO_3H; C) Pd/NUS-SO_3H; D) Pd/NUS; E) Catalytic performance of various catalysts. Reaction conditions: 5-HMF (1 mmol), catalyst (0.06 g), IPA (20 mL), temperature 150 °C, 2.0 MPa H_2; time 2 h.

nanoparticles, followed by etherification to 2,5-BIMF on SO_3H groups, and hydrogenolysis to 2-IMMF and 2,5-DMF on Pd nanoparticles.

After 2 h, Pd/NUS shows a 67.5 % conversion of 5-HMF, with 2.1 % selectivity to 2,5-DMF. Although Pd/NUS-SO_3H possesses a relatively lower BET surface area than Pd/UiO-SO_3H, it shows both the higher 5-HMF conversion (92.1 % vs. 67.5 %) and 2,5-DMF selectivity (52.8 % vs. 23.4 %) (Figure 3E). Over Pd/NUS-SO_3H, a 2,5-DMF yield of 95.2 % can be obtained after prolonging the reaction time to 6 h. Notably, tetrahydrofuranyl compounds (2,5-bishydroxymethyl tetrahydrofuran and its derivatives) obtained by furan ring hydrogenation were the most common side products in previous reports, and our catalytic system showed only trace amounts of them.[10,39,46,47] Pd/2D MOF-SO_3H clearly shows a superior catalytic performance in terms of conversion and selectivity than all reported catalysts, including porous or non-porous catalysts, with a higher concentration of 5-HMF, lower temperature and shorter reaction time, especially for these 3D catalysts containing metal and SO_3H sites (Table S3).[10,16,17,39,46–56]

Next, a variety of available monosaccharides (such as fructose and glucose), disaccharides (such as cellobiose and sucrose), and polysaccharides (such as inulin) were used as substrates. However, these saccharides are hard to dissolve in pure IPA solvent, resulting in inactive reactivity (Figure S10). Dimethyl sulfoxide (DMSO) is regarded as an effective solvent in saccharide conversion to 5-HMF owing to its advantages of dissolving saccharides and mediating fructose dehydration.[7] Therefore, direct conversion of saccharides to 2,5-DMF was carried out in a solvent mixture of DMSO and IPA. First, fructose reaction was conducted over Pd/UiO-SO_3H and Pd/NUS-SO_3H. With increasing reaction time, high-performance liquid chromatography (HPLC) showed a gradual decrease in fructose concentration, and gas chromatography (GC) showed that the concentrations of 5-HMF, 2,5-BHMF, 2,5-BIMF, and 2-IMMF first increased and then decreased (Figures 4A, B). After 6 h, fructose was completely converted, and Pd/UiO-SO_3H and Pd/NUS-SO_3H showed 2,5-DMF yields of 42.6 % and 90.2 %, respectively (Figure 4C). Fortunately, the carbon balance is more than 97 %, and no furan-hydrogenated or fructose-hydrogenated byproducts (i.e., tetrahydrofuranyl compounds and mannitol) can be detected. As far as we are aware, despite the higher fructose amount, lower temperature and shorter reaction time were used, the 2,5-DMF productivity of the catalytic system was still higher than all the previously reported reaction systems, including MOF-based or non-MOF-based catalysts (Table S4).[16–21,57] After removing the catalyst, the fructose conversion and 2,5-DMF selectivity remain unchanged, which illustrates that reaction is heterogeneously catalyzed by Pd/NUS-SO_3H and active sites cannot be leached (Figure S11). Furthermore, the spent catalyst was readily recovered. The reused Pd/NUS-SO_3H showed no obvious deactivation with the conversion of fructose and selectivity of 2,5-DMF after 4 recycles (Figure 4D). The PXRD, XPS, TEM, ICP-OES, and element analysis results showed its stable physicochemical structure under the reaction condition (Figure S12, Table S5).

Then, efficiency tests of Pd/NUS-SO_3H were carried out to upgrade other saccharides, e.g., glucose, sucrose, cellobiose, and inulin, to further integrate the hydrolysis of disaccharides and polysaccharides to monosaccharides and the isomerization of glucose to fructose. Compared to fructose, glucose was more difficult to upgrade because an extra isomerization step of glucose is a prerequisite of

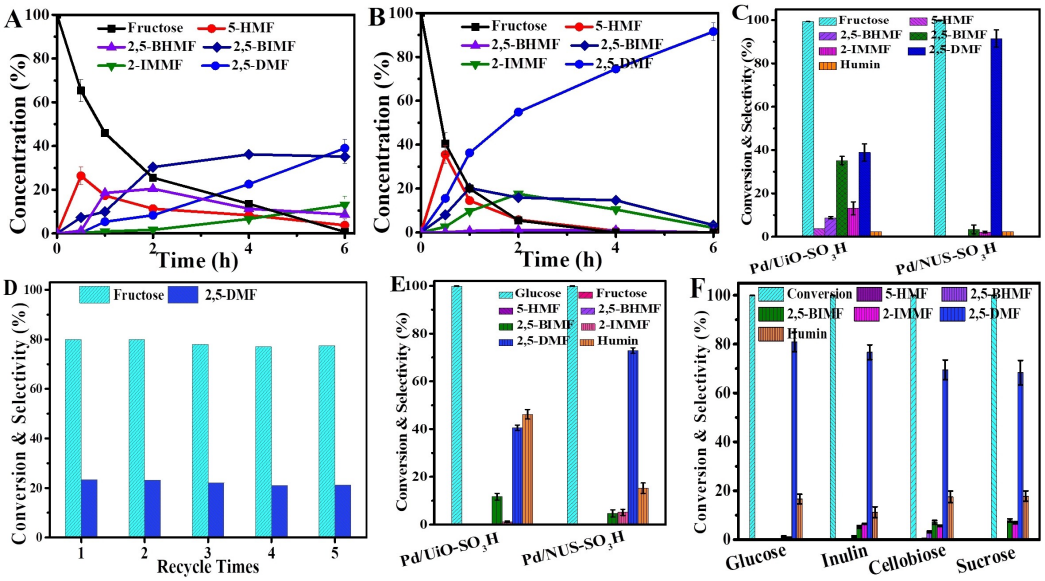

Figure 4. Time-dependent product concentration of fructose to 2,5-DMF over A) Pd/UiO-SO_3H and B) Pd/NUS-SO_3H; C) Catalytic performance of various catalysts for fructose reaction; D) Recycling performance of Pd/NUS-SO_3H for fructose reaction; E) Catalytic performance of various catalysts for glucose reaction; F) Catalytic results of various saccharides. Reaction conditions: catalyst (0.06 g), IPA (17 mL), DMSO (3 mL), temperature 150 °C, 2.0 MPa H_2; (A,B) fructose (1 mmol); C) fructose (1 mmol), 6 h; D) fructose (1 mmol), 1 h; E) glucose (1 mmol), 12 h; F) glucose (1 mmol), cellobiose (0.5 mmol, 0.171 g), sucrose (0.5 mmol, 0.171 g), inulin (0.171 g), 24 h.

dehydration and subsequent conversion. Meanwhile, a large amount of humins was easily generated by polymerization of reactive intermediates.[57] After 12 h, a 2,5-DMF yield of 72.9 % and carbon balance of 84.9 % are obtained over Pd/NUS-SO_3H, which are also superior to Pd/UiO-SO_3H (40.6 % and 54.8 %, respectively) (Figure 4E). Figure 4F summarizes the corresponding conversions of sugars and the yields of 2,5-DMF. A high 2,5-DMF yield of 76.7–90.2 % was obtained from fructose-united sugars (i.e., fructose and inulin). In contrast, sugars containing glucose units (i.e., glucose, sucrose, and cellobiose) exhibited slightly lower reactivity, and a prolonged reaction time of 24 h was required to achieve a 2,5-DMF yield of 68.3–80.8 %. These catalytic performances on these substrates are still unprecedentedly high (Table S6).[16,17,57] These results indicate that the 2D MOF-based catalyst also possesses a strong catalytic ability for various saccharides into 2,5-DMF.

To clearly identify the importance of Brønsted acidity, Pd/NUS and Pd/NUS-SO_3H were compared in fructose dehydration and 2,5-BHMF etherification under an N_2 atmosphere, and hydrogenolysis of 2,5-BIMF and 2-IMMF under an H_2 atmosphere, which are the most important reaction steps in 2,5-DMF synthesis (Figure 5A). Pd/NUS is rather inert, whereas Pd/NUS-SO_3H with a comparable Brønsted acid strength shows considerable activity. There is no doubt that SO_3H in the compact layers provides the site for the dehydration and etherification steps and activation of the ether groups for hydrogenolysis steps.[36,59] The role of the Lewis acidity was further studied by conducting a comparative experiment of Pd/C and Pd/NUS under an H_2 atmosphere. These products were verified by liquid chromatography-mass spectrometry (LC-MS) (Figure S13). The efficient synthesis of fructose-hydrogenated mannitol with 85.2 % selectivity over Pd/NUS and glucose-hydrogenated sorbitol with 83.1 % selectivity over Pd/C evidently indicate the susceptibility of glucose isomerization over the Lewis acidity of MOF (Figure 5B).[60,61] Meanwhile, the importance of Lewis acidity was also emphasized in 5-HMF hydrogenation. Indeed, Pd/NUS shows a 96.2 % selectivity of 2,5-BHMF, whereas Pd/C shows a 60.1 % selectivity of 2,5-bishydroxymethyl tetrahydrofuran (2,5-BTHMF) (Figure 5C). In situ attenuated total reflection infrared spectroscopy (ATR-IR) was used to elucidate the underlying molecular mechanism. When interacting with Pd/NUS and Pd/C, C=O group peaks redshifted from 1668 cm^{-1} to 1642 cm^{-1} over Pd/NUS, and to 1649 cm^{-1} over Pd/C (Figure 5D).[62,63] However, the position of the furan ring group is invariable at 1043 cm^{-1} over Pd/NUS, but redshifted to 1020 cm^{-1} over Pd/C. The results indicate that both the furan ring and C=O groups of 5-HMF are adsorbed, activated, and hydrogenated on the Pd/C surface, but only C=O group interact with MOF-based catalyst, which ensures the highly efficient preparation of 2,5-BHMF and inhibits the formation of BTHMF. This is consistent with previous work, which mentioned that the Lewis acid sites prefer to contact the electronegative O atom in asymmetric C=O rather than the symmetric C=C in the furan ring.[64] Hence, Lewis acidity not only provides the active sites for the

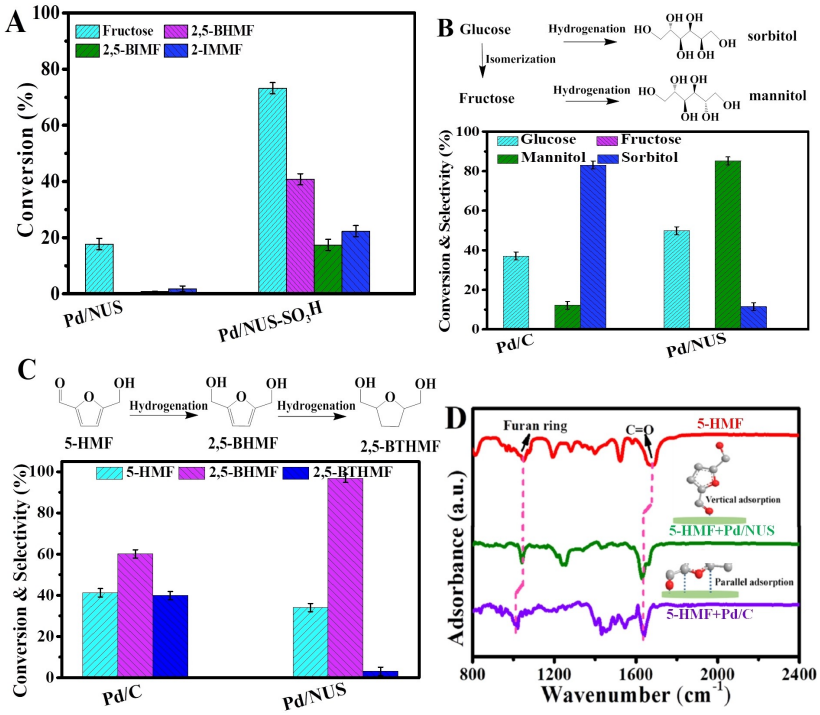

Figure 5. A) Catalytic performance of Pd/NUS and Pd/NUS-SO_3H of different reaction steps; catalytic performance of Pd/C and Pd/NUS for B) glucose hydrogenation reaction and C) 5-HMF hydrogenation reaction; D) ATR-IR spectra of 5-HMF adsorbed on different catalysts. Reaction conditions: substrate (1 mmol), catalyst (0.06 g), IPA (17 mL), DMSO (3 mL), temperature 150 °C, 2.0 MPa atmosphere; A) N_2 or H_2, 0.5 h, B), C) H_2, 0.5 h.

glucose reaction but also plays the role of a regulator for the selective hydrogenation of 5-HMF.

To appreciate the characteristic diffusion pathways of substrate, intermediates, and products from these composite catalysts, the time-of-flight secondary ion mass spectrometry (TOF-SIMS) depth profiling and chemical maps were employed.[65–67] The depth profiles and the reconstructed 3D images confirm S and Pd elements are concentrated near the external surface of Pd/UiO-SO_3H whereas a thick and dense slab of Zr and C elements (≈50 nm) is found in the MOF host (Figures 6A, B, S14). Although similar surface affinity for Pd and S is revealed in the Pd/NUS-SO_3H sample, it is interesting to note that a much thinner slab of 2D MOF (≈4 nm): the average distance between the Pd, SO_3H sites on the surface and Lewis acid sites (i.e., Zr) of Pd/NUS-SO_3H is much closer than that of Pd/UiO-SO_3H. To illustrate the difference in catalytic results, for the fructose and 5-HMF reaction, the reaction steps including fructose dehydration, 5-HMF hydrogenation, 2,5-BHMF etherification, 2,5-BIMF hydrogenolysis and 2-IMMF hydrogenolysis was conducted with Pd/NUS-SO_3H and Pd/UiO-SO_3H catalysts (Figure 6C). After 0.5 h, the fructose, 5-HMF, 2,5-BHMF, 2,5-BIMF, and 2-IMMF conversion rates follow the same order of Pd/NUS-SO_3H (20.4, 17.4, 27.6, 5.8, 7.4 mmol $g^{-1}h^{-1}$, respectively) > Pd/UiO-SO_3H (15.0, 12.0, 24.5, 5.0, 5.5 mmol $g^{-1}h^{-1}$, respectively), which result from the larger external specific surface area and higher exposure of SO_3H and metal sites of NUS-based catalyst.[38,59] Clearly, the hydrogenolysis step acts as the rate-determining step for the overall reaction. Over Pd/UiO-SO_3H, the generation rate of 2,5-DMF using fructose and 5-HMF as feedstocks (0.01 and 0.01 mmol $g^{-1}h^{-1}$, respectively) are lower than that using 2,5-BIMF as feedstock (3.5 mmol $g^{-1}h^{-1}$). However, over Pd/NUS-SO_3H, the generation rate of 2,5-DMF is reversed with an order of fructose (5.2 mmol $g^{-1}h^{-1}$) > 5-HMF (4.0 mmol $g^{-1}h^{-1}$) > 2,5-BIMF (3.7 mmol $g^{-1}h^{-1}$). In general, the generation rate of product from intermediate is faster than that from reactant. This observation over 2D MOF implies that the enhancement of intermediate diffusion can increase the overall conversion rate of the reaction. For the glucose reaction, the glucose conversion rate and 2,5-DMF generation rate over 2D MOF (15.0 and

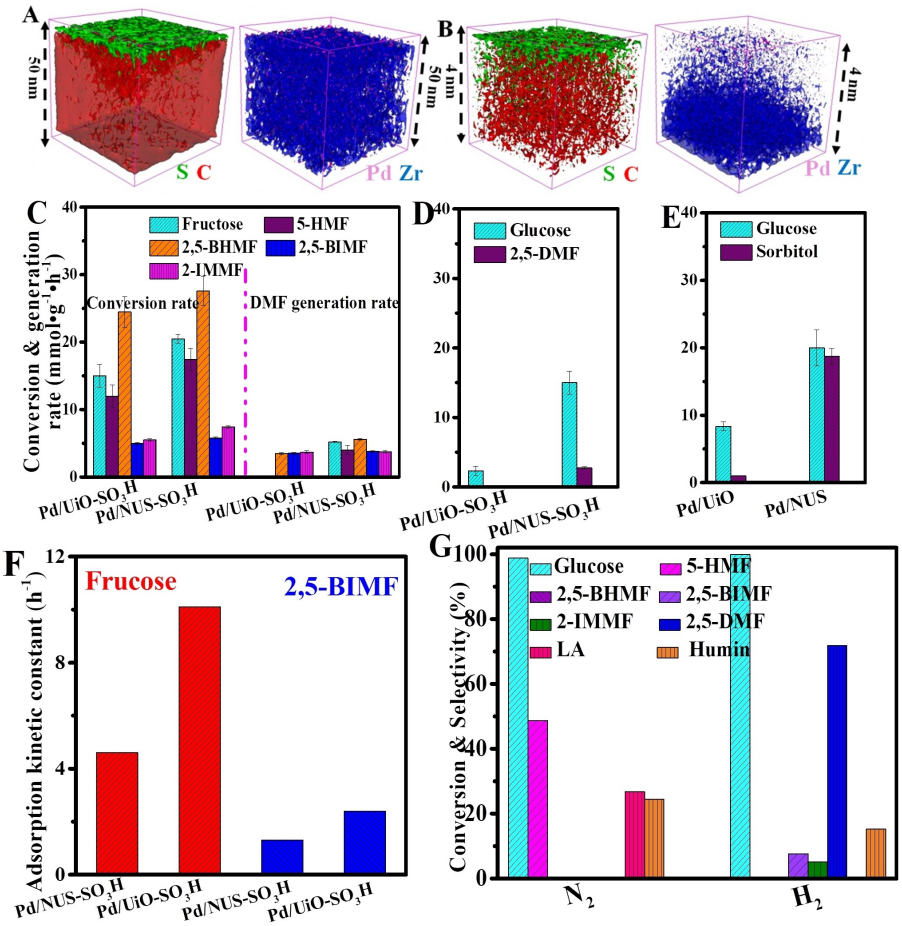

Figure 6. A) Negative (SO_3^-, C_6^-) and positive polarity (Pd^+, ZrO^+) ToF-SIMS 3D images of Pd/UiO-SO_3H and B) Pd/NUS-SO_3H; Conversion rate and 2,5-DMF generation rate of C) fructose, 5-HMF, 2,5-BHMF, 2,5-BIMF, 2-IMMF and D) glucose over Pd/NUS-SO_3H and Pd/UiO-SO_3H; E) glucose conversion rate and sorbitol generation rate of Pd/C and Pd/NUS; F) adsorption kinetic constant of fructose and 2,5-BIMF over Pd/UiO-SO_3H and Pd/NUS-SO_3H; G) Catalytic performance of Pd/NUS-SO_3H for glucose reaction under different atmosphere. Reaction conditions: substrate (1 mmol), catalyst (0.06 g), IPA (17 mL), DMSO (3 mL), temperature 150 °C. C)–E) 0.5 h, 2.0 MPa H_2; G) 12 h, 2.0 MPa N_2 or H_2.

2.7 mmol g^{-1} h^{-1}, respectively) are both much higher than those of 3DMOF (2.3 and 0.1 mmol g^{-1} h^{-1}, respectively) (Figure 6D). The microporous pore size of 2D MOF (1.5 nm) is accessible to glucose (1.01 × 0.66 × 0.61 nm) but that of 3DMOF is not, which implies that the Lewis site Zr^{4+} both in the edge and inside the pore takes effect in glucose isomerization over 2D MOF, while only the coordination-unsaturated Zr^{4+} in the edge of the 3DMOF crystal is effective.[30,38,43] The larger external specific surface area and wider pore size of 2D MOF cause a greater difference of the Lewis acid sites accessibility between 2D MOF and 3DMOF. The much faster isomerization reaction rate of 2D MOF was also verified by the glucose hydrogenation experiments over the Pd/MOF (Figure 6E), which indicates that glucose is preferred isomerized at the Lewis acid site of 2D MOF followed by hydrogenation, but directly hydrogenated at the metal sites of 3DMOF. To verify the difference in molecular diffusion of 2D MOF and 3DMOF, the adsorption of reprehensive reactant (fructose) and intermediate (2,5-BIMF) were measured under 30 °C (Figure S15). The adsorption kinetics of Pd/NUS-SO_3H and Pd/UiO-SO_3H follow first-order kinetics, which mean that the adsorption process was dominated by the diffusion process. Pd/NUS-SO_3H has faster adsorption rates than Pd/UiO-SO_3H due to the faster surface diffusion rate of the higher external specific surface area (Figures 6F, S15). Meanwhile, it possesses higher adsorption capacities due to the higher diffusion accessibility of larger microporous pore size. However, the adsorption rate of 2,5-BIMF is much lower than fructose. The higher 2,5-DMF productivity from 5-HMF and fructose than from 2,5-BIMF over Pd/NUS-SO_3H was reasonable owing to the much faster diffusion ability of 5-HMF than 2,5-BIMF, in which the in situ generated 2,5-BIMF at acidic sites can be rapidly transferred to hydrogenation sites for the hydrogenolysis step. On the other hand, over Pd/UiO-SO_3H, the multistep diffusion occurs at long-distance sites causes the lower 2,5-DMF generation rate. Then, the catalytic performance of the physical mixture of Pd/C and NUS-SO_3H with distant metal sites and acidic sites showed much lower 2,5-DMF productivity than Pd/NUS-SO_3H in fructose reaction, although they possess a similar dehydration rate (Figure S16). Based on these results, the rapid 2,5-DMF production over Pd/NUS-SO_3H can be attributed to the integration of cascade reaction steps by promoting the transmission of substrate and intermediates between different sites instead of reinforcing the elementary reaction rates. For the conversion of saccharides to 5-HMF under an N_2 atmosphere, large amounts of humins (24.5 %) and 5-HMF-hydrated levulinic acid (LA) (26.8 %) are generated on acidic sites by polymerization of active compounds and rehydration of 5-HMF, respectively (Figures 6G, S17).[7,11,12] However, the total yield (84.9 %) of 5-HMF (0.1 %) and their derivatives (2,5-BIMF 7.8 %, 2-IMMF 5.1 %, and 2,5-DMF 71.9 %) under an H_2 atmosphere are much higher than those of 5-HMF (48.7 %) under an N_2 atmosphere. The rapid conversion of 5-HMF to stable derivatives in the one-pot reaction systems can decrease the 5-HMF concentration and hinder the occurrence of unwanted side reactions by this powerful concerted catalysis.

Conclusion

It is challenging to develop new composite catalysts containing compact active sites at high density with desirable porosity to allow cascade reactions at high catalytic efficiency. We demonstrate that 2D MOF Pd/NUS-SO_3H shows an outstanding state-of-the-art catalytic performance for the one-pot conversion of saccharides into 2,5-DMF under mild reaction conditions. The characteristic ultrathin sheet structure of the 2D MOF possessing tailored catalytic functionalities in close contact with metal nanoparticles can largely facilitate the rapid transformation of reactants and intermediates over these various active sites, resulting in high generation efficiency. This work provides a powerful pathway for the direct production of 2,5-DMF from saccharides over multifunctional 2D MOF catalysts.

Acknowledgements

The authors appreciate the support from the National Natural Science Foundation of China (22178158, 52162014, 21878138, 22065024), the Cultivating Project for Academic and Technical Leader of Key Discipline of Jiangxi Province (20212BCJ23038), and the Special Fund of Jiangxi Graduate Student Innovation (YC2021-S130). Refinements of PXRD using TOPAS at University of Oxford, UK.

Conflict of Interest

The authors declare no conflict of interest.

Data Availability Statement

The data that support the findings of this study are available in the Supporting Information of this article.

Keywords: 2,5-Dimethylfuran · 5-Hydroxymethylfurfural · Multifunctional Catalysis · 2D metal-organic frameworks (MOFs) · Saccharides

[1] T. Thananatthanachon, T. B. Rauchfuss, *Angew. Chem. Int. Ed.* **2010**, *49*, 6616–6618; *Angew. Chem.* **2010**, *122*, 6766–6768.
[2] I. F. Teixeira, B. T. W. Lo, P. Kostetskyy, M. Stamatakis, L. Ye, C. C. Tang, G. Mpourmpakis, S. C. E. Tsang, *Angew. Chem. Int. Ed.* **2016**, *55*, 13061–13066; *Angew. Chem.* **2016**, *128*, 13255–13260.
[3] C. L. Williams, C. C. Chang, P. Do, N. Nikbin, S. Caratzoulas, D. G. Vlachos, R. F. Lobo, W. Fan, P. J. Dauenhauer, *ACS Catal.* **2012**, *2*, 935–939.
[4] M. Besson, P. Gallezot, C. Pinel, *Chem. Rev.* **2014**, *114*, 1827–1870.
[5] J. B. Binder, R. T. Rains, *J. Am. Chem. Soc.* **2009**, *131*, 1979–1985.
[6] P. P. Upare, D. W. Hwang, Y. K. Hwang, U. H. Lee, D. Y. Hong, J. S. Chang, *Green Chem.* **2015**, *17*, 3310–3313.

[7] Y. Román-Leshkow, J. N. Chheda, J. A. Dumesic, *Science* **2006**, *312*, 1933–1937.
[8] B. Saha, C. M. Bohn, M. M. Abu-Omar, *ChemSusChem* **2014**, *7*, 3095–3101.
[9] H. Li, C. Wang, Y. Xu, Z. Yu, S. Saravanamurugan, Z. Wu, S. Yang, R. Luque, *Green Chem.* **2020**, *22*, 637–645.
[10] Y. Román-Leshkow, C. J. Barrett, Z. Y. Liu, J. A. Dumesic, *Nature* **2007**, *447*, 982–985.
[11] Z. J. Wei, Y. X. Liu, T. Dilantha, Q. L. Ren, *Green Chem.* **2012**, *14*, 1220–1226.
[12] H. Ma, F. R. Wang, Y. H. Yu, L. F. Wang, X. H. Li, *Ind. Eng. Chem. Res.* **2015**, *54*, 2657–2666.
[13] Z. J. Wei, J. T. Lou, Z. B. Li, Y. X. Liu, *Catal. Sci. Technol.* **2016**, *6*, 6217–6225.
[14] M. Chidambaram, A. T. Bell, *Green Chem.* **2010**, *12*, 1253–1262.
[15] C. Zhu, H. Wang, C. Cai, K. Bi, B. Cai, X. Song, Q. Liu, L. Ma, *ACS Sustainable Chem. Eng.* **2019**, *7*, 16026–16040.
[16] J. Li, Z. Song, Y. Hou, Z. Li, C. Xu, C.-L. Liu, W.-S. Dong, *ACS Appl. Mater. Interfaces* **2019**, *11*, 12481–12491.
[17] R. Insyani, D. Verma, S. M. Kim, J. Kim, *Green Chem.* **2017**, *19*, 2482–2490.
[18] K. Ji, C. Shen, J. Yin, X. Feng, H. Lei, Y. Chen, N. Cai, T. Tan, *Ind. Eng. Chem. Res.* **2019**, *58*, 10844–10854.
[19] H. Li, W. Zhao, A. Riisager, S. Saravanamurugan, Z. Wang, Z. Fang, S. Yang, *Green Chem.* **2017**, *19*, 2101–2106.
[20] H. Li, W. Zhao, Z. Fang, *Appl. Catal. B* **2017**, *215*, 18–27.
[21] Y. Peng, Y. S. Li, Y. j Ban, H. Jin, W. M. Jiao, X. l Liu, W. S. Yang, *Science* **2014**, *346*, 1356–1359.
[22] T. Rodenas, I. Luz, G. Prieto, B. Seoane, H. Miro, A. Corma, F. Kapteijn, F. X. L. I. Xamena, J. Gascon, *Nat. Mater.* **2015**, *14*, 48–55.
[23] S. Zhao, Y. Wang, J. Dong, C. He, H. Yin, P. An, K. Zhao, X. Zhang, C. Gao, L. Zhang, J. Lv, J. Wang, J. Zhang, A. Khattak, N. A. Khan, Z. Wei, J. Zhang, S. Liu, H. Zhao, Z. Tang, *Nat. Energy* **2016**, *1*, 16184.
[24] C. He, K. Lu, D. Liu, W. Lin, *J. Am. Chem. Soc.* **2014**, *136*, 5181–5184.
[25] G. Lan, Z. Li, S. S. Veroneau, Y.-Y. Zhu, Z. Xu, C. Wang, W. Lin, *J. Am. Chem. Soc.* **2018**, *140*, 12369–12373.
[26] T. He, B. Ni, S. Zhang, Y. Gong, H. Wang, L. Gu, J. Zhuang, W. Hu, X. Wang, *Small* **2018**, *14*, 1703929.
[27] G. Lan, Y. Quan, M. Wang, G. T. Nash, E. You, Y. Song, S. S. Veroneau, X. Jiang, W. Lin, *J. Am. Chem. Soc.* **2019**, *141*, 15767–15772.
[28] Y. Guo, W. Shi, H. Yang, Q. He, Z. Zeng, J. Ye, X. He, R. Huang, C. Wang, W. Lin, *J. Am. Chem. Soc.* **2019**, *141*, 17875–17883.
[29] W. Shi, L. Cao, H. Zhang, X. Zhou, B. An, Z. Lin, R. Dai, J. Li, C. Wang, W. Lin, *Angew. Chem. Int. Ed.* **2017**, *56*, 9704–9709; *Angew. Chem.* **2017**, *129*, 9836–9841.
[30] Z. Hu, E. M. Mahdi, Y. Peng, Y. Qian, B. Zhang, N. Yan, D. Yuan, J.-C. Tan, D. Zhao, *J. Mater. Chem. A* **2017**, *5*, 8954–8963.
[31] Y. Huang, M. Zhao, S. Han, Z. Lai, J. Yang, C. Tan, Q. Ma, Q. Lu, J. Chen, X. Zhang, Z. Zhang, B. Li, B. Chen, Y. Zong, H. Zhang, *Adv. Mater.* **2017**, *29*, 1700102.
[32] S. He, Y. Chen, Z. Zhang, B. Ni, W. He, X. Wang, *Chem. Sci.* **2016**, *7*, 7101–7105.
[33] X. Zhang, P. Zhang, C. Chen, J. Zhang, G. Yang, L. Zheng, J. Zhang, B. Han, *Green Chem.* **2019**, *21*, 54–58.
[34] L. Cao, Z. Lin, F. Peng, W. Wang, R. Huang, C. Wang, J. Yan, J. Liang, Z. Zhang, T. Zhang, L. Long, J. Sun, W. Lin, *Angew. Chem. Int. Ed.* **2016**, *55*, 4962–4966; *Angew. Chem.* **2016**, *128*, 5046–5050.
[35] M. Lin Foo, S. Horike, T. Fukushima, Y. Hijikata, Y. Kubota, M. Takata, S. Kitagawa, *Dalton Trans.* **2012**, *41*, 13791–13794.
[36] Z. Hu, Y. Peng, Y. Gao, Y. Qian, S. Ying, D. Yuan, S. Horike, N. Ogiwara, R. Babarao, Y. Wang, N. Yan, D. Zhao, *Chem. Mater.* **2016**, *28*, 2659–2667.
[37] Y. Zhong, P. Zhang, X. Zhu, H. Li, Q. Deng, J. Wang, Z. Zeng, J.-J. Zou, S. Deng, *ACS Sustainable Chem. Eng.* **2019**, *7*, 14973–14981.
[38] S.-Y. Moon, Y. Liu, J. T. Hupp, O. K. Farha, *Angew. Chem. Int. Ed.* **2015**, *54*, 6795–6799; *Angew. Chem.* **2015**, *127*, 6899–6903.
[39] D. Wu, S. Zhang, W. Y. Hernández, W. Baaziz, O. Ersen, M. Marinova, A. Y. Khodakov, V. V. Ordomsky, *ACS Catal.* **2021**, *11*, 19–30.
[40] E. Yuan, C. Wu, X. Hou, M. Dou, G. Liu, G. Li, L. Wang, *J. Catal.* **2017**, *347*, 79–88.
[41] X. Gao, S. Tian, Y. Jin, X. Wan, C. Zhou, R. Chen, Y. Dai, Y. Yang, *ACS Sustainable Chem. Eng.* **2020**, *8*, 12722–12730.
[42] Y. Zhong, Q. Deng, Q. Yao, C. Lu, P. Zhang, H. Li, J. Wang, Z. Zeng, J.-J. Zou, S. Deng, *ACS Sustainable Chem. Eng.* **2020**, *8*, 7785–7794.
[43] J. H. Cavka, S. Jakobsen, U. Olsbye, N. Guillou, C. Lamberti, S. Bordiga, K. P. Lillerud, *J. Am. Chem. Soc.* **2008**, *130*, 13850–13851.
[44] F. Vermoortele, B. Bueken, G. Le Bars, B. Van de Voorde, M. Vandichel, K. Houthoofd, A. Vimont, M. Daturi, M. Waroquier, V. V. Speybroeck, C. Kirschhock, D. E. De Vos, *J. Am. Chem. Soc.* **2013**, *135*, 11465–11468.
[45] X. Feng, J. Hajek, H. S. Jena, G. Wang, S. K. P. Veerapandian, R. Morent, N. D. Geyter, K. Leyssens, A. E. J. Hoffman, V. Meynen, C. Marquez, D. E. De Vos, V. V. Speybroeck, K. Leus, P. V. D. Voort, *J. Am. Chem. Soc.* **2020**, *142*, 3174–3183.
[46] B. Hu, L. Warczinski, X. Li, M. Lu, J. Bitzer, M. Heidelmann, T. Eckhard, Q. Fu, J. Schulwitz, M. Merko, M. Li, W. Kleist, C. Hattig, M. Muhler, B. Peng, *Angew. Chem. Int. Ed.* **2021**, *60*, 6807–6815; *Angew. Chem.* **2021**, *133*, 6882–6891.
[47] G.-H. Wang, J. Hilgert, F. H. Richter, F. Wang, H.-J. Bongard, B. Spliethoff, C. Weidenthaler, F. Schüth, *Nat. Mater.* **2014**, *13*, 293–300.
[48] B. S. Solanki, C. V. Rode, *Green Chem.* **2019**, *21*, 6390–6406.
[49] J. Jae, W. Zheng, R. F. Lobo, D. G. Vlachos, *ChemSusChem* **2013**, *6*, 1158–1162.
[50] X. Wang, Y. Liu, X. Liang, *Green Chem.* **2018**, *20*, 2894–2902.
[51] Q. Wang, Z. Yu, J. Feng, P. Fornasiero, Y. He, D. Li, *ACS Sustainable Chem. Eng.* **2020**, *8*, 15288–15298.
[52] C. Zhu, H. Wang, H. Li, B. Cai, W. Lv, C. Cai, C. Wang, L. Yan, Q. Liu, L. Ma, *ACS Sustainable Chem. Eng.* **2019**, *7*, 19556–19569.
[53] B. Chen, F. Li, Z. Huang, G. Yuan, *Appl. Catal. B* **2017**, *200*, 192–199.
[54] A. B. Gawade, M. S. Tiwari, G. D. Yadav, *ACS Sustainable Chem. Eng.* **2016**, *4*, 4113–4123.
[55] Y. Zu, P. Yang, J. Wang, X. Liu, J. Ren, G. Lu, Y. Wang, *Appl. Catal. B* **2014**, *146*, 244–248.
[56] T. Gan, Y. Liu, Q. He, H. Zhang, X. He, H. Ji, *ACS Sustainable Chem. Eng.* **2020**, *8*, 8692–8699.
[57] R. Insyani, D. Verma, H. S. Cahyadi, S. M. Kim, S. K. Kim, N. Karanwal, J. Kim, *Appl. Catal. B* **2019**, *243*, 337–354.
[58] L. Wang, H. Wang, F. Liu, A. Zheng, J. Zhang, Q. Sun, J. P. Lewis, L. Zhu, X. Meng, F. Xiao, *ChemSusChem* **2014**, *7*, 402–406.
[59] N. Yan, Y. Yuan, R. Dykeman, Y. Kou, P. J. Dyson, *Angew. Chem. Int. Ed.* **2010**, *49*, 5549–5553; *Angew. Chem.* **2010**, *122*, 5681–5685.
[60] W. Yin, Z. Tang, R. H. Venderbosch, Z. Zhang, C. Cannilla, G. Bonura, F. Frusteri, H. J. Heeres, *ACS Catal.* **2016**, *6*, 4411–4422.
[61] X. Zhang, L. J. Durndell, M. A. Isaacs, C. M. A. Parlett, A. F. Lee, K. Wilson, *ACS Catal.* **2016**, *6*, 7409–7417.

[62] Q. Deng, J. Zhu, Y. Zhong, X. Li, J. Wang, J. Cai, Z. Zeng, J.-J. Zou, S. Deng, *ACS Sustainable Chem. Eng.* **2021**, *9*, 11127–11136.
[63] X. Li, L. Zhang, Q. Deng, S. Chen, J. Wang, Z. Zeng, S. Deng, *ChemSusChem* **2022**, *15*, e202102532.
[64] M. Zhao, K. Yuan, Y. Wang, G. Li, J. Guo, L. Gu, W. Hu, H. Zhao, Z. Tang, *Nature* **2016**, *539*, 76–80.
[65] J. Zhu, W. Li, R. Huang, L. Ma, H. Sun, J.-H. Choi, L. Zhang, Y. Cui, G. Zou, *J. Am. Chem. Soc.* **2020**, *142*, 16276–16284.
[66] I. H. Abidi, L.-T. Weng, C. P. J. Wong, A. Tyagi, L. Gan, Y. Ding, M. Li, Z. Gao, R. Xue, M. D. Hossain, M. Zhuang, X. Ou, Z. Luo, *Chem. Mater.* **2018**, *30*, 1718–1728.
[67] Z. Ristanović, J. P. Hofmann, U. Deka, T. U. Schülli, M. Rohnke, A. M. Beale, I. B. M. Weckhuysen, *Angew. Chem. Int. Ed.* **2013**, *52*, 13382–13386; *Angew. Chem.* **2013**, *125*, 13624–13628.

Manuscript received: April 13, 2022
Accepted manuscript online: June 14, 2022
Version of record online: July 13, 2022